



Investigation on C–TiO₂ nanotubes composite as Pt catalyst support for methanol electrooxidation

Xu-Lei Sui ^{a,b}, Zhen-Bo Wang ^{a,*}, Min Yang ^a, Li Huo ^a, Da-Ming Gu ^b, Ge-Ping Yin ^a

^a School of Chemical Engineering and Technology, Harbin Institute of Technology, No. 92 West-Da Zhi Street, Harbin 150001, China

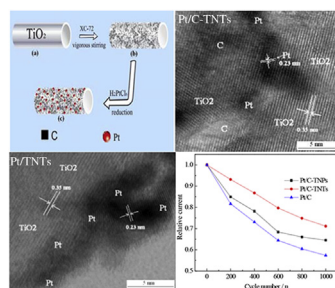
^b School of Science, Harbin Institute of Technology, No. 92 West-Da Zhi Street, Harbin 150001 China



HIGHLIGHTS

- A convenient approach to prepared Pt/C–TiO₂ nanotubes (TNTs) via a microwave-assisted polyol process.
- Carbon-coated TNTs possess three-phase position which is conducive to deposit Pt nanoparticles.
- The higher electronic conductivity of TNTs is more beneficial to exhibit performance of platinum.
- The enhanced activity and stability of Pt/C–TNTs is attributed to the combination of carbon and TNTs.

GRAPHICAL ABSTRACT



ARTICLE INFO

Article history:

Received 24 October 2013

Received in revised form

2 December 2013

Accepted 1 January 2014

Available online 8 January 2014

Keywords:

Titania nanotubes

Direct methanol fuel cell

Platinum catalyst

Stability

ABSTRACT

In this paper, Pt nanoparticles have been successfully deposited on the mixture of carbon black and one-dimensional self-ordered TiO₂ nanotubes (TNTs) array by a microwave-assisted polyol process to synthesize Pt/C–TNTs catalyst. TiO₂ nanoparticles (TNPs) are used instead of TNTs to prepare catalyst as a reference. The obtained samples are characterized by physical characterization and electrochemical measurements. The results show that Pt nanoparticles are uniformly deposited on the three-phase interfaces between carbon and TNTs. The Pt/C–TNTs possesses substantially enhanced activity and stability in electrochemical performance. Such remarkable properties are due to the excellent composite carrier of C–TNTs: (1) TNTs has strong corrosion resistance in acidic and oxidative environment and a metal support interaction between Pt and TNTs; (2) Compared to TNPs, TNTs is more suitable for electrocatalytic field on account of its better electronic conductivity; (3) Compared to TNPs, TNTs can improve the anti-poisoning ability of catalyst for methanol oxidation. (4) Amorphous carbon can improve the dispersion of platinum particles; (5) The distribution of carbon improves the poor conductivity of TNTs. These studies indicate that Pt/C–TNTs compound is a promising catalyst for methanol electrooxidation.

© 2014 Elsevier B.V. All rights reserved.

1. Introduction

At present, Pt-based materials are the most widely used catalysts for methanol electrooxidation in direct methanol fuel cells

(DMFC). To obtain a high surface area, Pt nanoparticles have been synthesized, supported and mixed with different carbon materials including carbon black [1–7], carbon nanotube [8–11], carbon fiber [12–15], graphene [16–19], and hollow core/mesoporous shell carbon [20,21]. However, the carbon support degrades over time due to electrochemical corrosion causes the migration and agglomeration of Pt nanoparticles, decreasing the stability of Pt/C catalyst [22–24]. In addition, it is demonstrated that the active Pt

* Corresponding author. Tel.: +86 451 86417853.

E-mail address: wangzb@hit.edu.cn (Z.-B. Wang).

nanoparticles can catalyze and accelerate carbon corrosion [25]. To improve the stability of support, Numerous attempts are underway on the addition of metal oxide supports such as WO_3 [26], SnO_2 [27], TiO_2 [28–34], CeO_2 [35,36], SiO_2 [37] and so on.

So far, titania has attracted increasing attention due to its low cost, environmental friendliness and high corrosion resistance in acidic environment [29,38]. Furthermore, titania can enhance catalytic activity of platinum due to a metal-support interaction (MSI) [39,40] between titania and platinum. However, there is one major problem to restrict its application in fuel cell that titania is a semiconducting metal oxide. To address the question, TiO_2 -based composites have been investigated recently, such as TiO_2 -carbon [30,41], TiO_2 -MCNTs [42], TiO_2 - MoO_3 [43], TiO_2 - CeO_2 [44]. Since the first report on the growth of self-ordered TiO_2 nanotubes (TNTs) array by electrochemical anodization [32], this kind of novel one-dimensional nanostructure have been gained extremely attentions due to the high aspect ratio, excellent charge transport, large specific surface area and good mechanical strength. Therefore, many applications of TNTs were explored in photocatalysts, solar cells, electrochromic devices and biosensors [45,46]. In the two main crystal phases of TiO_2 , it was reported that electron transfer is about 10 times faster in anatase than in rutile [47], which means the electronic properties of TNTs can be modified by annealing conditions [48].

As we know, the microwave-assisted polyol process (MAPP) is a promising method for preparing Pt-based catalyst [49,50] and in our recent work TiO_2 nanoparticles (TNPs) were used as a composite supported Pt nanoparticles by microwave-assisted polyol process (MAPP) to improve catalyst durability [30,42,51]. In order to improve conductivity and surface area of catalyst support, here TNTs replaced TNPs as an attractive catalyst support for proton exchange membrane fuel cell. In our work, Pt/C-TNPs, Pt/TNTs and Pt/C-TNTs compounds were prepared via MAPP and characterized by accelerated durability test (ADT), X-ray diffraction (XRD), energy dispersive analysis of X-ray (EDAX), transmission electron microscopy (TEM) and X-ray photoelectron spectroscopy (XPS). Compared to no catalytic activity of Pt/TNPs [30], Pt/TNTs showed catalytic activity to a certain extent, demonstrating that TNTs possess better electronic conductivity. Moreover, the addition of carbon further improves the conductivity of material and makes the distribution of Pt nanoparticles more uniform. In addition, Pt/C-TNTs compound exhibits significantly excellent catalytic activity and stability compared to commercial Pt/C catalyst.

2. Experimental

2.1. Materials preparation

2.1.1. Preparation of TiO_2 nanotube

To fabricate of self-organized TNTs, Ti foils were degreased by sonicating in acetone, isopropanol, and methanol, rinsed with deionized water and dried in air. Anodization was carried out in a two-electrode system with a counter of Pt sheet. TNTs were grown in an ethylene glycol electrolyte containing 0.1 mol L^{-1} NH_4F and 1 mol L^{-1} H_2O at 50 V for 3 h. After anodization, samples were washed with deionized water and dried in N_2 , then placed in the couple annealing at 400 °C for 2 h and cooled to room temperature.

2.1.2. Preparation of Pt/carbon– TiO_2 nanotube catalyst

Pt-based catalyst with the Pt loading of 20 wt.% was synthesized by microwave-assisted polyol process in ethylene glycol (EG) solution with H_2PtCl_6 as precursor salt. Briefly, 20 mg TNTs (or TNPs) and 30 mg Vulcan XC-72 carbon black were dispersed into the mixed solution of 25 mL containing EG and isopropyl alcohol (V/V = 4:1) in 150 mL beaker under ultrasonic treatment for 1 h to

form uniform suspension, then 1.68 mL of 0.038 mol L^{-1} H_2PtCl_6 -EG solution with a subsequent stirring process for 3 h. The pH value of the suspension was adjusted by adding 1 mol L^{-1} NaOH -EG solution dropwise to 12.0. Then argon gas was fed into the suspension for 15 min to expel oxygen with a subsequent microwave heating process for 40 s to fix Pt on carbon-coated TNTs support. The suspension was allowed to cool down to room temperature with continuous stirring, and then the pH value was adjusted to 2–3 by HNO_3 aqueous solution. The mixture was kept stirring for 12 h and then the product was washed repeatedly with ultrapure water (Millipore, 18.2 MΩ cm) until no Cl^- ions were detected. Lastly, the obtained Pt/C-TNTs catalyst was dried for 3 h at 80 °C in a vacuum oven and then stored in a vacuum vessel. All chemicals used were of analytical grade. At the same time, the Pt/TNTs catalyst with the Pt loading of 20 wt.% was prepared for comparison.

2.1.3. Preparation of working electrode

The catalyst ink was prepared by ultrasonically dispersing 5.0 mg catalyst in 2.5 mL ultrapure water and the dispersion was then ultrasonicated for 20 min. The glassy carbon (GC) working electrode with 4 mm of diameter was polished with $0.05 \mu\text{m}$ alumina suspensions to a mirror finish before each experiment and served as an underlying substrate of the working electrode. A certain amount (the Pt loading of $32 \mu\text{g cm}^{-2}$ on GC for sulfuric acid test system and $16 \mu\text{g cm}^{-2}$ on GC for sulfuric acid methanol test system) of the dispersion was pipetted out on the top of the GC and onto which 5 μL of a dilute aqueous Nafion® solution (5 wt. % solution in a mixture of lower aliphatic alcohols and ultrapure water) was applied.

2.2. Electrochemical measurements

Electrochemical measurements were carried out in a conventional sealed three-electrode electrochemical cell at 25 °C. A piece of Pt foil (1 cm^2) and a mercurous sulfate electrode (MSE, 0.64 V relative to normal hydrogen electrode, NHE) were used as the counter and reference electrodes, respectively. The working electrode was the glass carbon electrode which was made by the above mentioned procedure. The solution of 0.5 mol L^{-1} H_2SO_4 and 0.5 mol L^{-1} H_2SO_4 containing 0.5 mol L^{-1} CH_3OH was purged with ultrapure argon gas for 20 min under constantly stirring before starting the experiment. The cyclic voltammograms (CV) were carried out within a potential range from –0.64 to 0.51 V with CHI650A electrochemical analysis instrument controlled by an IBM PC. Electrochemical impedance spectra (EIS) were usually obtained at frequencies between 100 kHz and 0.01 Hz with 12 points per decade. The amplitude of the sinusoidal potential signal was 5 mV. In order to get rid of the possible contaminations caused by Nafion® film, the working electrode was treated by continuously cycling at a scan rate of 0.05 V s^{-1} until a stable response was obtained before the measurement curves were recorded. Fresh electrolyte solution was used for each time electrochemical measurement in order to ensure repeated results. All potentials are reported vs MSE in the paper. All chemicals used were of analytical grade, and solution was prepared with ultrapure water.

The accelerated durability test (ADT) is a fast way to evaluate the stability of a catalyst. In this work, the stability of the catalyst was considered by the ADT which was conducted by cycling the potential between –0.64 and 0.51 V in 0.5 mol L^{-1} H_2SO_4 at a scan rate of 0.05 V s^{-1} .

The electrochemical active specific surface area (ESA) of platinum can be calculated with coulombic charges accumulated during hydrogen adsorption or desorption after correcting for the double-layer charging current from the CVs [11,30]:

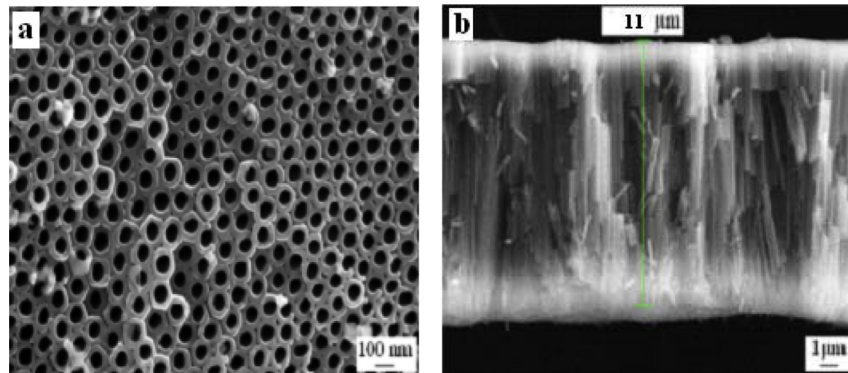


Fig. 1. SEM images of TNTs (a) top-view (b) cross-section.

$$ESA = \frac{Q_H}{0.21 \text{ mC} \cdot \text{cm}^{-2} \times M_{\text{Pt}}} \quad (1)$$

where Q_H (mC) is the charge due to the hydrogen adsorption/desorption in the hydrogen region of the CVs, 0.21 mC cm^{-2} is the electrical charge associated with monolayer adsorption of hydrogen on Pt, and M_{Pt} is the loading of Pt metal on the working electrode.

2.3. Characterizations of physical properties

2.3.1. Scanning electron microscopy (SEM)

Morphological characterization of the TNTs sample was carried out by scanning electron microscope (SEM, Zeiss SUPRA 55).

2.3.2. X-ray diffraction (XRD)

XRD data was collected by the D/max-RB diffractometer (made in Japan) using a Cu Ka X-ray source operating at 45 kV and 100 mA, scanning at a rate of 4° min^{-1} with an angular resolution of 0.05° of the 2θ scan.

2.3.3. Energy dispersive analysis of X-ray (EDAX)

The elemental compositions of the samples were investigated by EDAX. Hitachi-S-4700 analyzer was connected to a scanning electron microscope (SEM, Hitachi Ltd. S-4700). The samples were supported on aluminum foils to remove the influence of the conductive carbon tape, and then the incident electron beam energies impinged the sample surface from the normal angle for 100 s with energies ranging from 3 to 30 keV.

2.3.4. Transmission electron microscopy (TEM) and high resolution transmission electron microscopy (HRTEM)

TEM and HRTEM were carried out by a Japan JEOLJEM-2010EX transmission electron microscope with a spatial resolution of 1 nm. The applied voltage was 100 kV. Before taking the electron micrographs, the catalyst samples were ultrasonically dispersed in alcohol, and a drop of the resultant dispersion was deposited and dried on a standard copper grid coated with a polymer film.

2.3.5. X-ray photoelectron spectroscopy (XPS)

XPS analysis was carried out to determine the surface properties of the catalysts using a Physical Electronics PHI model 5700 instrument, with Al X-ray source operating at 250 W. The takeoff angle of the sample to analyzer was 45° . Survey spectra were collected at pass energy (PE) of 187.85 eV over a binding energy range from 0 to 1300 eV. High binding energy resolution multiplex data for the individual elements were collected at a PE of 29.55 eV. During all XPS experiments, the pressure inside the vacuum system

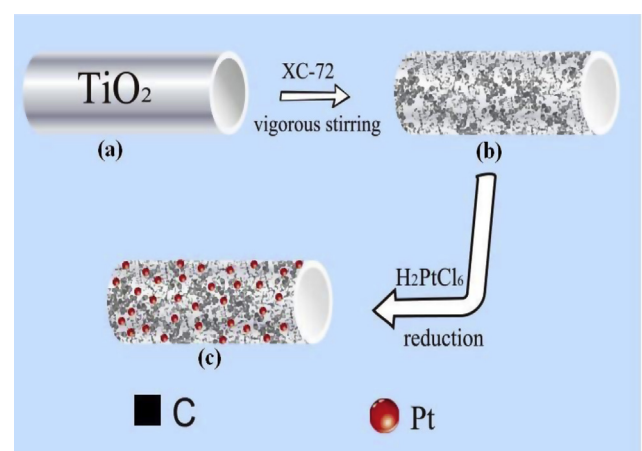
was maintained at 1×10^{-9} Pa. Before the above analysis, all samples were dried under vacuum at 80°C overnight.

3. Results and discussion

Fig. 1 shows SEM images of as-formed (amorphous) TNTs by anodization. From the top view in Fig. 1a, as-formed TNTs is highly self-organized and with diameter of 30–40 nm (Fig. 1a). The gaps between the individual tubes are formed and nanotubes are compact and well-attached. The aligned TNTs length shown in Fig. 1b is approximately 11 μm and it can be easily controlled by anodization time. After annealing at 400°C for 2 h, the TNTs is ready for the subsequent experiments.

Scheme 1 is the preparation process of Pt/C–TNTs catalyst. **Scheme 1(a)** shows TNTs obtained via anodization and sintering process. Through ultrasonic dispersion and vigorous stirring in polyol system, one part of carbon (Vulcan XC-72) is uniformly distributed on the surface of TNTs as shown in **Scheme 1(b)**, another part of carbon is dispersed in the gap of TNTs. The carbon among TNTs plays a role of good link, while the carbon on the surface of TNTs causes the generation of three-phase interface, corresponding with the junction space of TNTs and carbon as shown in **Scheme 1(b)**. Because the three-phase interface is conducive to deposit platinum nanoparticles [30], the Pt nanoparticles are uniformly deposited on the boundaries of the mixed supports as shown in **Scheme 1(c)**.

Fig. 2 shows the XRD patterns of TNTs (a), Pt/TNTs (b), Pt/C–TNTs (c) and Pt/C–TNPs (d), respectively. Spectrum (a)



Scheme 1. Schematic diagram of the Pt catalyst preparation process.

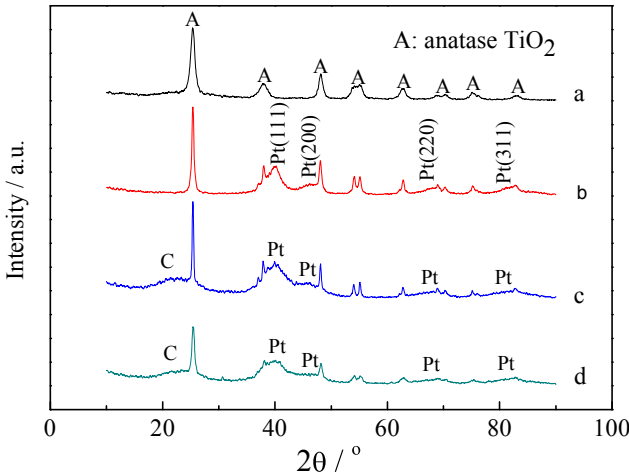


Fig. 2. XRD patterns of TNTs (a), Pt/TNTs (b), Pt/C-TNTs (c) and Pt/C-TNPs (d).

demonstrates that TNTs are perfect anatase phase. The representative diffraction peaks of Pt [(111), (200), (220) and (311)] shown in spectrum (b, c and d) indicate that Pt metal is subsistent in the form of a face-centered cubic (f.c.c.) phase structure. The influence of TiO_2 strong peaks makes Pt peaks concealed partly, however, the peak of Pt (111) is distinctly observed. The bases of patterns (c) and (d) are unstable because of the existence of carbon. Compared to patterns (c) and (d), the similarity illustrates a consistent crystal structure.

From the EDAX analysis in Fig. 3, the elemental peak of Pt is distinct in all samples, and the Pt mass contents are 18.7%, 18.4% and 20.8% in Pt/C-TNPs (a), Pt/C-TNTs (b) and Pt/TNTs (c), similar to the theoretical value of 20%. That indicates that chloroplatinic acid is almost completely reduced to Pt metal.

TEM images and associated size distributions of Pt/C-TNPs, Pt/C-TNTs and Pt/TNTs before and after ADT are shown in Fig. 4. It is clearly seen from Fig. 4a and c that the distributions of Pt nanoparticles of Pt/C-TNPs and Pt/C-TNTs are both more uniform than that of Pt/TNTs shown in Fig. 4e, which is assignable to the fact that the presence of carbon augments the deposition of Pt nanoparticles. The mean sizes of Pt nanoparticles of Pt/C-TNPs and Pt/C-TNTs are almost the same of 2.7 nm. As to Fig. 4b and d, it can be distinctly seen that the crystallite sizes of Pt/C-TNPs and Pt/C-TNTs grow to 4.3 nm and 4.4 nm after 1000 cycles ADT, increasing by 1.6 nm and 1.7 nm. The results of TEM are consistent with the results of electrochemical measurements discussed below. In addition, tubular morphology is clearly observed in Fig. 4c and e.

HRTEM images of Pt/C-TNTs and Pt/TNTs are shown in Fig. 5a and b. The lattice spacing of 0.35 nm and 0.23 nm is clearly seen which is attributed to the (101) plane of the anatase TiO_2 and the (111) plane of face centered cubic (f.c.c.) Pt, respectively. In addition, some amorphous phase in Fig. 5a is found and is ascribed to carbon. It can also be distinctly observed that the Pt nanoparticles of Pt/C-TNTs are uniformly distributed on the boundaries of carbon and TNTs, while the Pt nanoparticles of Pt/TNTs agglomerate on TNTs, further demonstrating that the presence of carbon is conducive to the dispersion of Pt nanoparticles.

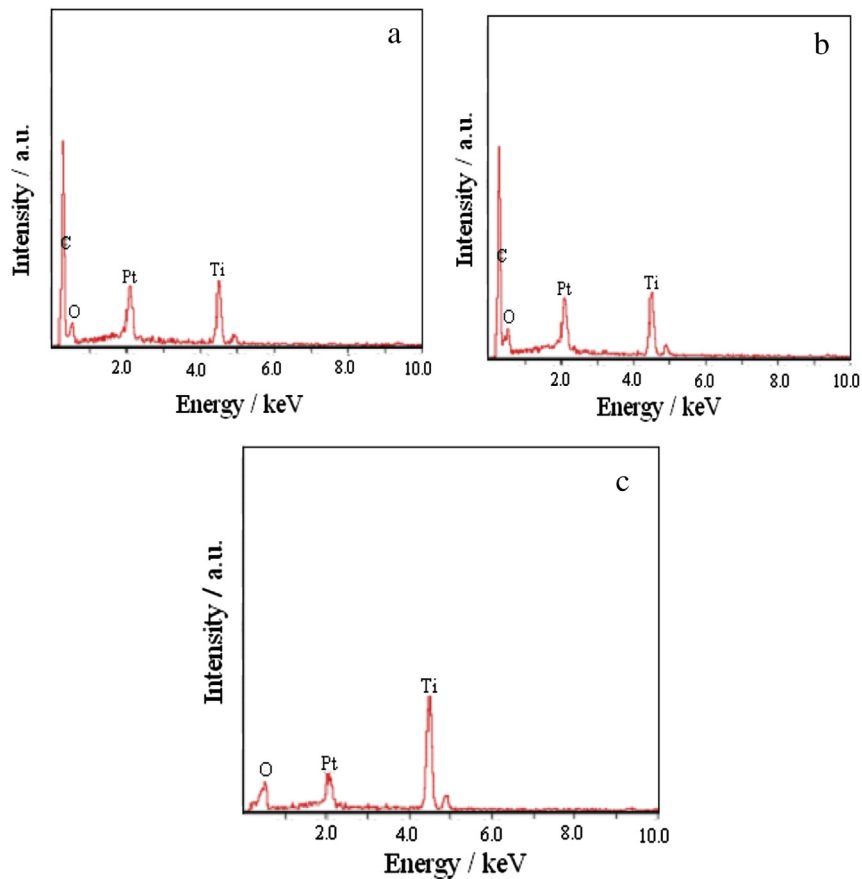


Fig. 3. EDAX patterns of Pt/C-TNPs (a), Pt/C-TNTs (b) and Pt/TNTs (c).

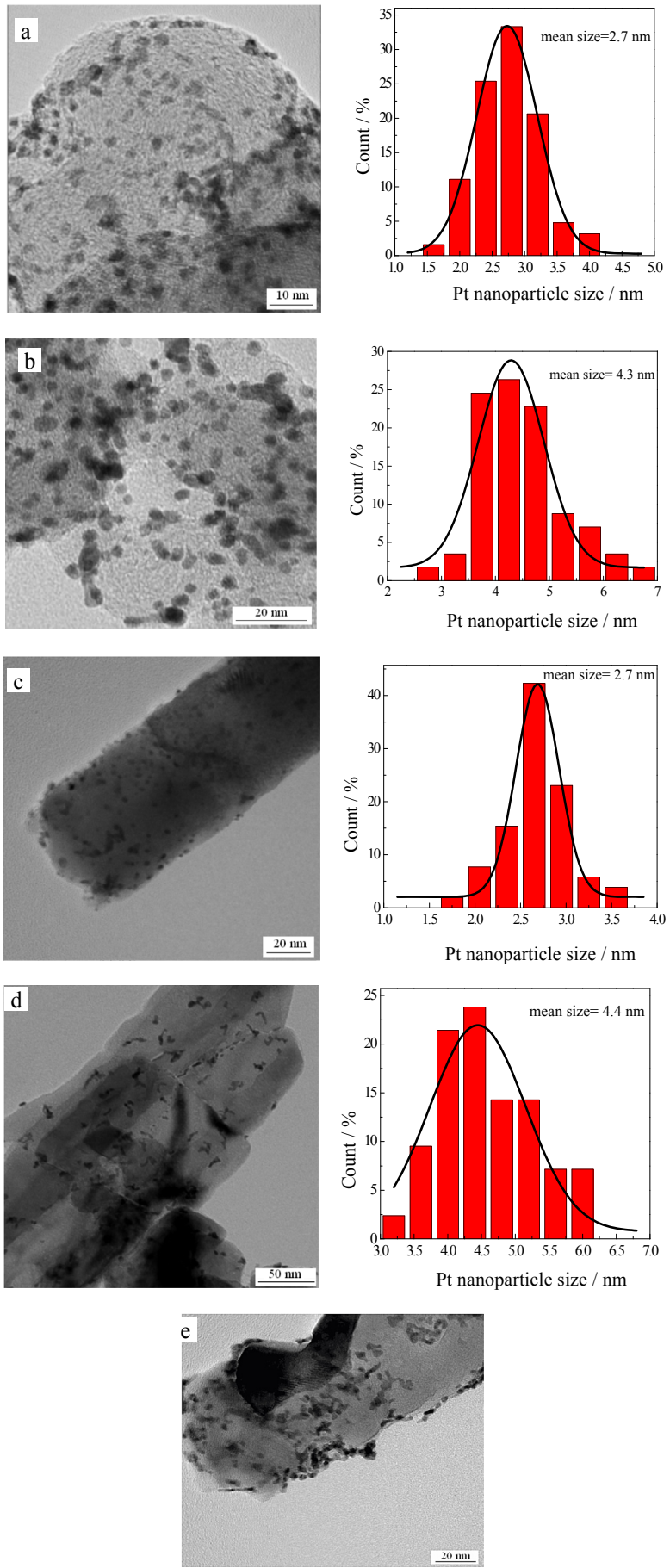


Fig. 4. TEM images and the size distributions of Pt/C-TNPs (a, b), Pt/C-TNTs (c, d) and Pt/TNTs (e) before (a, c, e) and after (b, d) ADT.

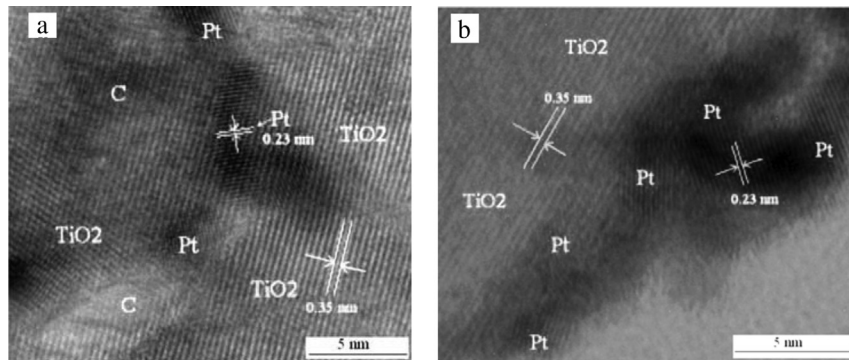


Fig. 5. HRTEM images of Pt/C-TNTs (a) and Pt/TNTs (b).

X-ray photoelectron spectroscopy (XPS) is an efficient method to analyze chemical state information of elements. As shown in Fig. 6a derived from XPS analysis, Pt4f peaks of Pt/C-TNPs and Pt/C-TNTs are substantially the same, not only in the shape but also in the position of peaks. This confirms that platinum in these two catalysts has a similar composition of valence. To gain further the ratio of different valence, the curve fitting of Pt4f peak for Pt/C-TNTs and Pt/C-TNPs is carried out and the result is shown in Fig. 6b and c and Table 1. The Pt (0) content of Pt/C-TNTs and Pt/C-TNPs is similar, respectively 46.6% and 49.3%. Compared with our previous work [30,52], the content of Pt (0) is analogous, while the content of Pt (IV) is too much. This can be interpreted as the oxidation of numerous unstable Pt (II) due to prolonged exposure in the air. Moreover, the binding energy of Pt (0) for Pt/C-TNTs and Pt/C-TNPs shows a shift up of 0.55 eV and 0.65 eV in comparison with that of Pt/C [52]. Because the mean size of Pt nanoparticles and the content of Pt(0) in the Pt/C-TNTs catalyst are very similar to Pt/C [52], the shift of binding energy of Pt(0) indicates further the metal-

support interaction (MSI) between Pt nanoparticles and titanium oxide.

Cyclic voltammograms (CV) for Pt/C-TNPs, Pt/C-TNTs, commercial Pt/C, Pt/TNTs and Pt/TNPs as well as ADT of Pt/C-TNPs, Pt/C-TNTs and Pt/C are carried out in 0.5 mol L⁻¹ H₂SO₄ at 25 °C and the results are shown in Fig. 7. Electrochemically active specific surface areas (ESA) of Pt nanoparticles are obtained by measurements of the hydrogen adsorption–desorption (HAD) integrals. The variations of ESA during the ADT are shown in Fig. 7e and f. In contrast with Pt/TNPs that there is no characteristic HAD region of Pt in Fig. 7a, CV of Pt/TNTs presents characteristic HAD region of Pt, which demonstrates that the conductivity of TNTs is better than TNPs. The improved electrical conductivity is also proved by Myung [53] and Zhang [54] used four-point probe measuring system. However, the ESA of Pt/TNTs only reaches 22.1 m² g⁻¹_{Pt} that is far less than 89.7 m² g⁻¹_{Pt} of Pt/C-TNTs, which is ascribed to two major factors: (1) the addition of carbon further increases the electronic conductivity of support; (2) the addition of carbon

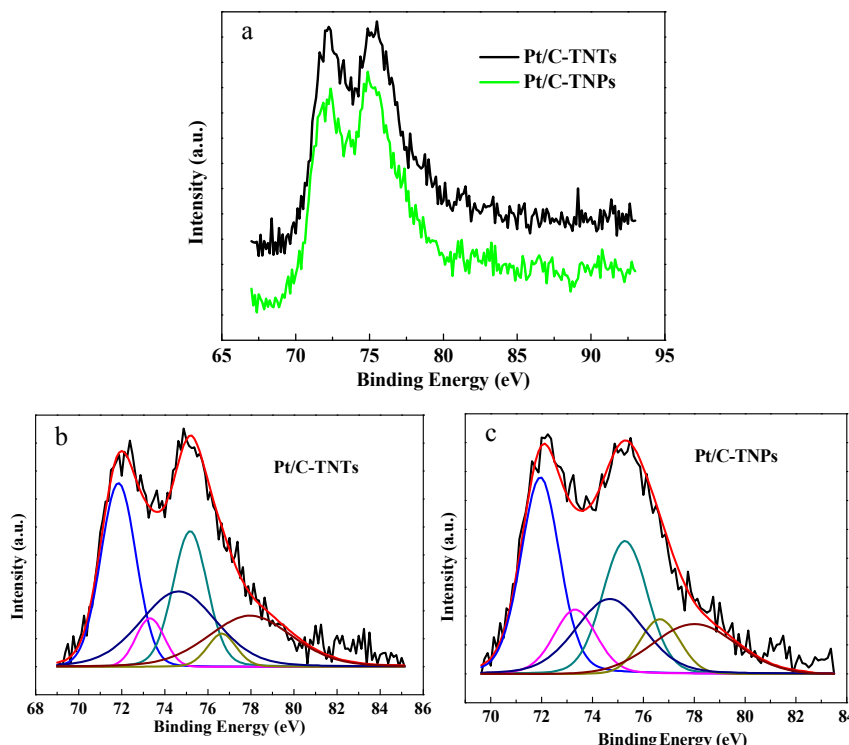


Fig. 6. Pt4f peaks of Pt/C-TNPs and Pt/C-TNTs (a); the curve fitting of Pt4f peak for Pt/C-TNTs (b) and Pt/C-TNPs (c).

Table 1

Results of the fit of the Pt4f peak, values given in % of the total intensity.

Sample	Pt species	Binding energy/eV	Relative concentration/%
Pt/C-TNPs	Pt (0)	71.95	49.3
	Pt (II)	73.32	17.7
	Pt (IV)	74.68	33.0
Pt/C-TNTs	Pt (0)	71.85	46.6
	Pt (II)	73.32	9.7
	Pt (IV)	74.64	43.8

improves the dispersion of Pt nanoparticles that can be seen from the TEM images. In addition, the ESA of Pt/C-TNTs is higher than $82.1 \text{ m}^2 \text{ g}^{-1} \text{ Pt}$ of Pt/C-TNPs and $56.3 \text{ m}^2 \text{ g}^{-1} \text{ Pt}$ of commercial Pt/C. Because the mean size and dispersion of platinum particles in two of them are very similar, the small improvement of ESA may be attributed to the better conductivity of TNTs mentioned above. From Fig. 7e and f, it can be seen that ESA of Pt/C-TNTs is always higher than that of Pt/C-TNPs and commercial Pt/C. After 1000 cycles, their ESA losses by 36.6%, 33.4% and 42.5%, respectively. Overall, Pt/C-TNTs catalyst shows better electrochemical activity and stability, compared with those of the commercial Pt/C one.

Fig. 8a shows the CV curves of methanol electrooxidation on Pt/C-TNPs, Pt/C-TNTs and commercial Pt/C catalysts in an Ar-saturated solution of $0.5 \text{ mol L}^{-1} \text{ H}_2\text{SO}_4$ containing 0.5 mol L^{-1}

CH_3OH at a scanning rate of 50 mV s^{-1} at 25°C . It can be seen that the peak current density of Pt/C-TNTs is higher. The performance improvement may be ascribed to the reason that the metal support interaction and the better electronic conductivity of TNTs reduces the reaction internal resistance. The long-time stability behavior of Pt/C-TNPs, Pt/C-TNTs and commercial Pt/C catalysts toward methanol electrooxidation is evaluated, and the results of cycling aging test are shown in Fig. 8b–d. From the normalized peak current density as presented in Fig. 8e, it can be seen that the relative peak current for methanol electrooxidation on Pt/C-TNTs after 1000 cycles is higher than Pt/C-TNPs and commercial Pt/C. Their retention rates of peak currents are 71.1%, 64.5% and 57.3%, respectively. It is noteworthy that the stability behavior of Pt/C-TNPs and Pt/C-TNTs in methanol is different from that in H_2SO_4 . Such result indicates that the Pt/C-TNTs catalyst has better anti-poisoning for methanol electrooxidation.

Electrochemical impedance spectroscopy (EIS) is an effective measurement to determine the charge transfer resistance, which reflects the activity of a catalyst for methanol electrooxidation. The Nyquist plot (a) and Bode plot (b) of methanol electrooxidation in an Ar-saturated solution of $0.5 \text{ mol L}^{-1} \text{ CH}_3\text{OH}$ and $0.5 \text{ mol L}^{-1} \text{ H}_2\text{SO}_4$ at 25°C on Pt/C-TNPs and Pt/C-TNTs catalysts at 600 mV are shown in Fig. 9. It is well known that the slow kinetics is caused by the intermediate CO_{ads} from methanol dehydrogenation, which is strongly adsorbed on Pt sites to block continuous adsorption and

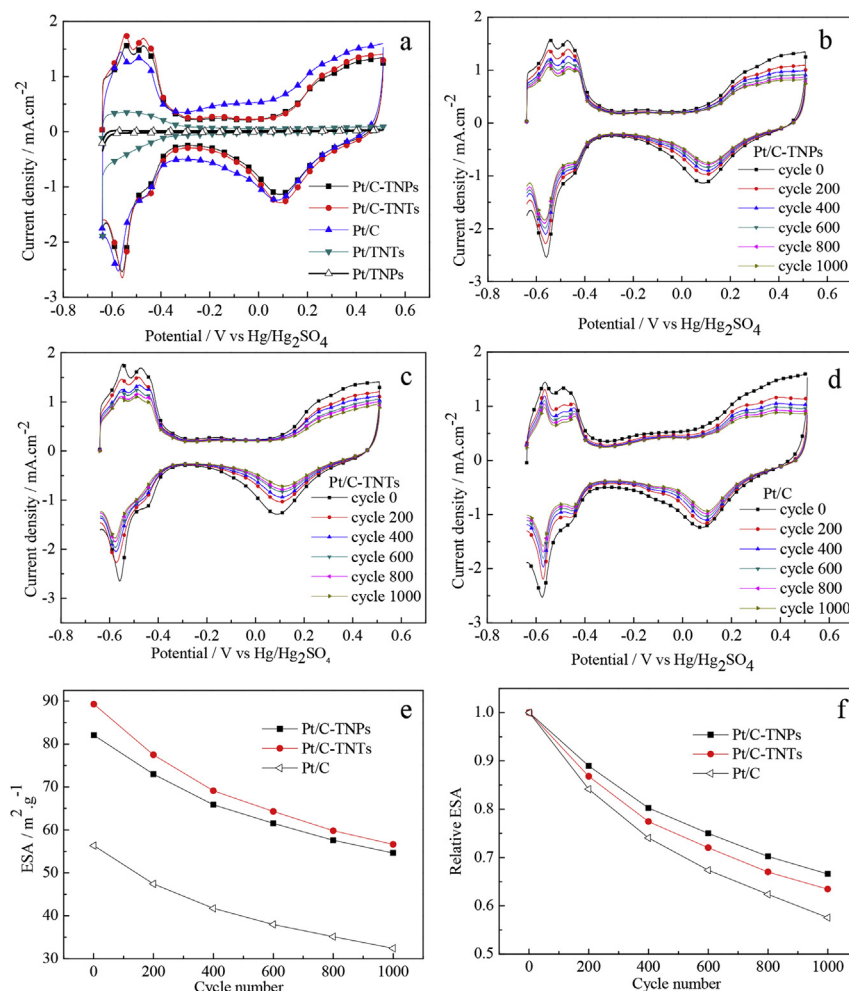


Fig. 7. CV for Pt/C-TNPs, Pt/C-TNTs, commercial Pt/C, Pt/TNTs and Pt/TNPs (a); ADT of Pt/C-TNPs (b), Pt/C-TNTs (c) and commercial Pt/C (d); relationship of ESA and cycle number during ADT (e, f). Scanning rate: 50 mV s^{-1} ; test temperature: 25°C ; solution: $0.5 \text{ mol L}^{-1} \text{ H}_2\text{SO}_4$.

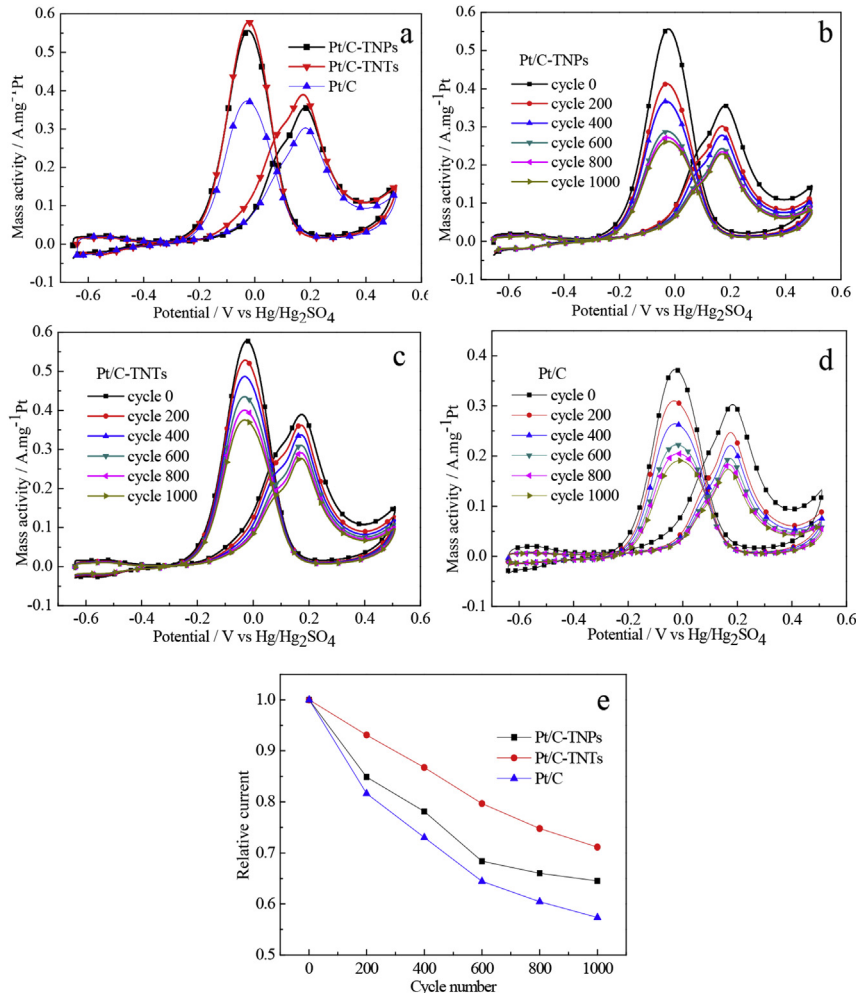


Fig. 8. CV of methanol electrooxidation for Pt/C-TNPs, Pt/C-TNTs and commercial Pt/C (a); cycling aging of Pt/C-TNPs (b), Pt/C-TNTs (c) and commercial Pt/C (d); relationship of normalized peak current density and cycle number (e). Scanning rate: 50 mV s⁻¹; test temperature: 25 °C; solution: 0.5 mol L⁻¹ H₂SO₄ containing 0.5 mol L⁻¹ CH₃OH.

dehydrogenation of methanol molecules [55–58]. It can be seen from Fig. 9a that the semicircle of Pt/C-TNTs is smaller than Pt/C-TNPs, indicating that the electrooxidation rate on Pt/C-TNTs is much faster than Pt/C-TNPs. In other words, the CO poisoning on the Pt active sites is being decreased by using TNTs instead of TNPs. The result is similar to that of cycling aging test in methanol. The amplified part of Nyquist plot at high frequency regions is inserted

in Fig. 9a. The internal resistances (curves intersect X-axis) of Pt/C-TNPs and Pt/C-TNTs catalysts are evidently different. The internal resistance of Pt/C-TNTs catalyst is lower than that of Pt/C-TNPs. Such result indicates that TNTs has better electronic conductivity, as is consistent with that of CV. The change of the rate-determining step of methanol electrooxidation can be obtained through the Bode plot. The Bode plots of Pt/C-TNPs and Pt/C-TNTs catalysts in

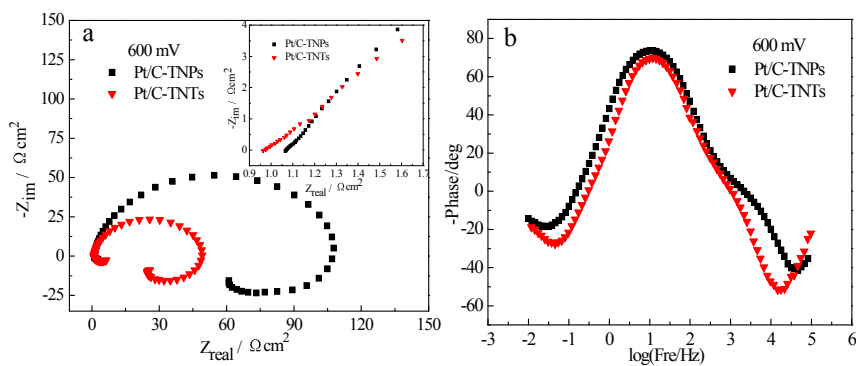


Fig. 9. Nyquist plot (a) and Bode plot (b) of methanol electrooxidation in an Ar-saturated solution of 0.5 mol L⁻¹ CH₃OH and 0.5 mol L⁻¹ H₂SO₄ at 25 °C on Pt/C-TNPs and Pt/C-TNTs catalyst at 600 mV; Inserted picture: amplified parts at high frequency regions.

Fig. 9b are similar, indicating that the rate-determining steps of methanol electrooxidation are both same. Therefore, the comparison of reaction impedance on Pt/C–TNPs and Pt/C–TNTs is more significant.

4. Conclusion

In summary, Pt/C–TNTs composite was prepared by a microwave-assisted polyol process and was characterized respectively by physical and electrochemical measurements. These studies have shown that the composite material of C–TNTs possesses a lot of three-phase interfaces. The Pt/C–TNTs served as highly efficient catalysts in the methanol electrooxidation reaction with better activity and durability than those of the Pt/C–TNPs and the commercial Pt/C. The enhanced performance could be attributed to the combined features of amorphous carbon and TNTs. The results reported herein suggest that superior catalysts can be developed by designing the structure and composition of the supports.

Acknowledgment

This research is financially supported by the National Natural Science Foundation of China (Grant No. 21273058 and 21203043), China Postdoctoral Science Foundation (Grant No. 2012M520731 and 2012M520729) and Heilongjiang Postdoctoral Financial Assistance (LBH-Z12089).

References

- [1] C.L. Hui, X.G. Li, I.M. Hsing, *Electrochim. Acta* 51 (2005) 711–719.
- [2] Q.L. Jiang, Z.D. Peng, X.F. Xie, K. Du, G.R. Hu, Y.X. Liu, *Trans. Nonferrous Met. Soc. China* 21 (2011) 127–132.
- [3] D.Y. Zhang, Z.F. Ma, G.X. Wang, J. Chen, G.C. Wallace, H.K. Liu, *Catal. Lett.* 122 (2008) 111–114.
- [4] C.P. Liu, X.Z. Xue, T.H. Lu, W. Xing, *J. Power Sources* 161 (2006) 68–73.
- [5] X.W. Yu, S.Y. Ye, *J. Power Sources* 172 (2007) 133–144.
- [6] W. Li, X.S. Zhao, T. Cochell, A. Manthiram, *Appl. Catal. B Environ.* 129 (2013) 426–436.
- [7] T. Cochell, W. Li, A. Manthiram, *J. Phys. Chem. C* 117 (2013) 3865–3873.
- [8] X. Wang, W.Z. Li, Z.W. Chen, M. Waje, Y.S. Yan, *J. Power Sources* 158 (2006) 154–159.
- [9] W.Z. Li, C.H. Liang, W.J. Zhou, J.S. Qiu, Z.H. Zhou, G.Q. Sun, Q. Xin, *J. Phys. Chem. B* 107 (2003) 6292–6299.
- [10] Y.Y. Mu, H.P. Liang, J.S. Hu, L. Jiang, L.J. Wan, *J. Phys. Chem. B* 109 (2005) 22212–22216.
- [11] Y.C. Xing, *J. Phys. Chem. B* 108 (2004) 19255–19259.
- [12] L. Deng, S.J. Guo, M. Zhou, L. Liu, C. Liu, S.J. Dong, *Biosens. Bioelectron.* 25 (2010) 2189–2193.
- [13] H.X. Huang, S.X. Chen, C. Yuan, *J. Power Sources* 175 (2008) 166–174.
- [14] D. Sebastian, I. Suelves, R. Moliner, M.J. Lazaro, A. Stassi, V. Baglio, A.S. Arico, *Appl. Catal. B Environ.* 132 (2013) 22–27.
- [15] D. Sebastian, I. Suelves, E. Pastor, R. Moliner, M.J. Lazaro, *Appl. Catal. B Environ.* 132 (2013) 13–21.
- [16] R. Siburian, T. Kondo, J. Nakamura, *J. Phys. Chem. C* 117 (2013) 3635–3645.
- [17] R. Siburian, J. Nakamura, *J. Phys. Chem. C* 116 (2012) 22947–22953.
- [18] C.T. Hsieh, Y.Y. Liu, D.Y. Tzou, W.Y. Chen, *J. Phys. Chem. C* 116 (2012) 26735–26743.
- [19] D.P. He, Y.L. Jiang, H.F. Lv, M. Pan, S.C. Mu, *Appl. Catal. B Environ.* 132 (2013) 379–388.
- [20] J. Zeng, C. Francia, C. Gerbaldi, M.A. Dumitrescu, S. Specchia, P. Spinelli, *J. Solid State Electrochem.* 16 (2012) 3087–3096.
- [21] B. Ficicilar, A. Bayrakceken, I. Eroglu, *Int. J. Hydrogen Energy* 35 (2010) 9924–9933.
- [22] K.H. Kangasniemi, D.A. Condit, T.D. Jarvi, *J. Electrochem. Soc.* 151 (2004) E125–E132.
- [23] E. Guilmot, A. Corcella, M. Chatenet, F. Maillard, F. Charlot, G. Berthome, C. Iojoiu, J.Y. Sanchez, E. Rossinot, E. Claude, *J. Electrochem. Soc.* 154 (2007) B1106–B1114.
- [24] J.J. Wang, G.P. Yin, Y.Y. Shao, S. Zhang, Z.B. Wang, Y.Z. Gao, *J. Power Sources* 171 (2007) 331–339.
- [25] L.M. Roen, C.H. Paik, T.D. Jarvi, *Electrochim. Solid State Lett.* 7 (2004) A19–A22.
- [26] N. Muthuraman, P.K. Guruvaiah, P.G. Agneeswara, *Mater. Chem. Phys.* 133 (2012) 924–931.
- [27] A. Kowal, S.L. Gojkovic, K.S. Lee, P. Olszewski, Y.E. Sung, *Electrochim. Commun.* 11 (2009) 724–727.
- [28] C.T. Lin, H.J. Huang, J.J. Yang, M.H. Shiao, *Microelectron. Eng.* 88 (2011) 2644–2646.
- [29] S.Y. Huang, P. Ganeshan, S. Park, B.N. Popov, *J. Am. Chem. Soc.* 131 (2009) 13898.
- [30] Z.Z. Jiang, Z.B. Wang, Y.Y. Chu, D.M. Gu, G.P. Yin, *Energy Environ. Sci.* 4 (2011) 728–735.
- [31] L.H. Yu, J.Y. Xi, *Electrochim. Acta* 67 (2012) 166–171.
- [32] V. Zwilling, E. Darque-Ceretti, A. Boutry-Forveille, D. David, M.Y. Perrin, M. Aucouturier, *Surf. Interface Anal.* 27 (1999) 629–637.
- [33] G. Wu, M.A. Nelson, N.H. Mack, S.G. Ma, P. Sekhar, F.H. Garzon, P. Zelenay, *Chem. Commun.* 46 (2010) 7489–7491.
- [34] C.S. Chen, F.M. Pan, *Appl. Catal. B Environ.* 91 (2009) 663–669.
- [35] Y.-Y. Chu, Z.-B. Wang, Z.-Z. Jiang, D.-M. Gu, G.-P. Yin, *Adv. Mater.* 23 (2011) 3100–3104.
- [36] D.M. Gu, Y.Y. Chu, Z.B. Wang, Z.Z. Jiang, G. Yin, Y. Liu, *Appl. Catal. B Environ.* 102 (2011) 9–18.
- [37] H.N. Yang, S.H. Cho, W.J. Kim, *J. Membr. Sci.* 421 (2012) 318–326.
- [38] Z.M. Liu, J.L. Zhang, B.X. Han, J.M. Du, T.C. Mu, Y. Wang, Z.Y. Sun, *Microporous Mesoporous Mater.* 81 (2005) 169–174.
- [39] T.T.H. Van, C.J. Pan, J. Rick, W.N. Su, B.J. Hwang, *J. Am. Chem. Soc.* 133 (2011) 11716–11724.
- [40] S.J. Yoo, T.Y. Jeon, K.S. Lee, K.W. Park, Y.E. Sung, *Chem. Commun.* 46 (2010) 794–796.
- [41] J. Ma, A. Habrioux, N. Guignard, N. Alonso-Vante, *J. Phys. Chem. C* 116 (2012) 21788–21794.
- [42] Z.Z. Jiang, Z.B. Wang, W.L. Qu, D.M. Gu, G.P. Yin, *Appl. Catal. B Environ.* 123 (2012) 214–220.
- [43] S. Zafeiratos, G. Papakonstantinou, M.M. Jacksic, S.G. Neophytides, *J. Catal.* 232 (2005) 127–136.
- [44] S. Kundu, J. Ciston, S.D. Senanayake, D.A. Arena, E. Fujita, D. Stacchiola, L. Barrio, R.M. Navarro, J.L.G. Fierro, J.A. Rodriguez, *J. Phys. Chem. C* 116 (2012) 14062–14070.
- [45] P. Roy, S. Berger, P. Schmuki, *Angew. Chem. Int. Ed.* 50 (2011) 2904–2939.
- [46] I. Paramasivam, H. Jha, N. Liu, P. Schmuki, *Small* 8 (2012) 3073–3103.
- [47] H. Tang, K. Prasad, R. Sanjines, P.E. Schmid, F. Levy, *J. Appl. Phys.* 75 (1994) 2042–2047.
- [48] A. Tighineanu, T. Ruff, S. Albu, R. Hahn, P. Schmuki, *Chem. Phys. Lett.* 494 (2010) 260–263.
- [49] W.X. Chen, J.Y. Lee, Z.L. Liu, *Chem. Commun.* (2002) 2588–2589.
- [50] Z.L. Liu, J.Y. Lee, W.X. Chen, M. Han, L.M. Gan, *Langmuir* 20 (2004) 181–187.
- [51] Z.Z. Jiang, Z.B. Wang, Y.Y. Chu, D.M. Gu, G.P. Yin, *Energy Environ. Sci.* 4 (2011) 2558–2566.
- [52] Z.Z. Jiang, Z.B. Wang, D.M. Gu, E.S. Smotkin, *Chem. Commun.* 46 (2010) 6998–7000.
- [53] S.T. Myung, M. Kikuchi, C.S. Yoon, H. Yashiro, S.J. Kim, Y.K. Sun, B. Scrosati, *Energy Environ. Sci.* 6 (2013) 2609–2614.
- [54] C.K. Zhang, H.M. Yu, Y.K. Li, W. Song, B.L. Yi, Z.G. Shao, *Electrochim. Acta* 80 (2012) 1–6.
- [55] N. Wagner, E. Gulzow, *J. Power Sources* 127 (2004) 341–347.
- [56] I.M. Hsing, X. Wang, Y.J. Leng, *J. Electrochem. Soc.* 149 (2002) A615–A621.
- [57] M. Ciureanu, H. Wang, *J. Electrochem. Soc.* 146 (1999) 4031–4040.
- [58] G. Wu, L. Li, B.Q. Xu, *Electrochim. Acta* 50 (2004) 1–10.